Fluorescence Probe Studies on the Structure of the Adsorbed Layer of Dodecyl Sulfate at the Alumina–Water Interface

PREM CHANDAR,* P. SOMASUNDARAN,* AND NICHOLAS J. TURRO†

*Henry Krumb School of Mines and †Department of Chemistry, Columbia University, New York, New York 10027

Received April 8, 1986; accepted July 31, 1986

Pyrene and dinaphthylpropane (DNP) fluorescence probes were used to investigate the structure of the adsorbed layer of sodium dodecyl sulfate at the alumina–water interface. The fluorescence fine structure of pyrene yielded information on the polarity of the microenvironment in the adsorbed layer. Intramolecular excimer formation of DNP was used to measure the microviscosity of this environment. The results indicate the presence of highly organized surfactant aggregates at the solid–liquid interface, formed by the association of hydrocarbon chains. Fluorescence decay methods enabled the determination of the size of these aggregates and their evolution as a function of surface coverage. The overall spectroscopic investigation reveals a molecular model that is in agreement with the concept of hemimicellization.

INTRODUCTION

Adsorption of ionic surfactants on charged particulate solids has been the subject of considerable research owing to the fundamental importance of it to many applications like flotation (1), detergency (2), enhanced oil recovery (3), and lubrication (4). Conventionally, adsorption studies involve the determination of adsorption isotherms, zeta potentials, particle wettability, and heats of adsorption (5). The analysis of these results has provided an understanding of surfactant adsorption in terms of the major mechanisms governing the formation of the adsorbed layer. In particular, electrostatics and surfactant association at the solid–liquid interface have been established as important interactions in ionic surfactant-charged solid systems (6). However, information on the structure of the adsorbed layer is lacking, largely due to the unavailability of spectroscopic techniques capable of directly probing the solid–liquid interface on a molecular level. Techniques such as infrared spectroscopy (7) and ellipsometry (8) involve *ex situ* procedures such as freezing, drying, *in vacuo*, etc., and/or have necessitated the use of ideal surfaces. Clearly these methods have limited applicability for studying surfactant adsorption on particulate solids in aqueous media.

Advances in fluorescence spectroscopy have enabled the use of organic fluorescent probes for *in situ* characterization of molecular environments such as surfactant micelles (9). The utility of fluorescence methods in such studies arises from the fact that the fluorescence responses of numerous probes are highly environment dependent so that specific information may be obtained by the appropriate choice of probes. Fluorescence responses that have been shown to depend on micellar environment include excitation and emission spectra, decay rates, quantum yields of emission, fluorescence polarization, and quenching (or sensitization) (10). These responses have been, in turn, related to molecular properties such as polarity, viscosity, diffusion, solute partitioning, and aggregation numbers, from which information on the dynamic and physical aspects of micellization has been obtained (11).

In contrast, few studies have reported the use of fluorescence probes to investigate sur-

0021-9797/87 $3.00

factant adsorption on solid substrates. Levitz *et al.* (12) recently demonstrated that steady-state emission and fluorescence decay techniques can be used to obtain structural information on adsorbed surfactant layers at the solid–liquid interface. In the present work, similar methods were utilized to characterize the structure of the adsorbed layer formed by an anionic surfactant (dodecyl sulfate) on a positively charged oxide (alumina). In particular, the polarity, microviscosity (rigidity), and size (aggregation number) of the surfactant microenvironment in the adsorbed layer were determined. These results were correlated with the adsorption and zeta potential behavior of the system in order to elucidate the formation and growth of the adsorbed layer as a function of surface coverage.

PRINCIPLES

The evidence accumulated in the literature suggests that the structure of surfactant adsorbed layers is, in some respects, analogous to that of surfactant micelles. Hence fluorescence techniques that are used to elucidate specific structural details of micelles can be used to characterize the adsorbed layer. In the present study, specific fluorescence probing methods were used to determine structural properties such as polarity, microviscosity and surfactant aggregation numbers of the adsorbed layer. The principles of these techniques, which are well-established in studies of micelle structure, are discussed below.

Steady-State Emission of Pyrene: Polarity of Microenvironment

The pyrene fluorescence fine structure has been found to be markedly dependent on the solvent (13). In particular the intensities of the first ($I1$) and the third ($I3$) vibrionic bands at 373 and 383 nm, respectively, are sensitive to the solvent polarity (14). In practice, the intensity ratio, $I3/I1$, is measured in solvents of known polarity and the polarity of the unknown environment is determined using this information. Typically $I3/I1$ for pyrene changes from ~0.6 in water to >1 in hydrocarbon media (13e). Pyrene has been widely utilized as a polarity probe in the study of surfactant micelles since owing to its hydrophobic nature, pyrene is selectively solubilized in micelles (15). The fluorescence response in an aqueous micellar solution thus reflects the polarity of the micelle media. $I3/I1$ values measured in various micelles range from 0.7 to 1.0 (13e). These polarities, which are intermediate between hydrocarbon and aqueous environments, have been considered to be due to water penetration in the micelle inner layers (where pyrene is reportedly located) (16). More recently, Mukerjee has considered the solubilization of aromatics in micelles (16d) in terms of a "two-state" model. Accordingly, these intermediate polarities can be interpreted as being due to an equilibrium distribution of pyrene between the micelle–water interface (adsorbed state) and micelle core (dissolved state).

Levitz *et al.* (12) found that pyrene was strongly solubilized in the adsorbed layer of Triton X-100 on silica. They measured a polarity that was similar to that of pyrene in Triton X-100 micelles from which they concluded that the surfactant environment in the adsorbed layer was formed by surfactant association in a manner analogous to micellization.

Fluorescence Decay of Analysis of Pyrene Excimer Formation: Surfactant Aggregation Numbers

Pyrene excimer formation has been studied extensively in homogeneous solutions as well as in micellar solutions (17). A homogeneous solution is an example of an infinite (or continuous) medium, while a micellar solution is an example of a fragmented medium; this distinction is based on the differences in the dynamics of excimer formation within these two types of environments (12).

An excimer forms when an excited state pyrene P^* interacts with a ground state pyrene P to form P_2^*:

$$P \xrightarrow{+h\nu} P^* \xrightarrow{k_0} P + h\nu$$
$$P + P^* \xrightarrow{k_e'} P_2^* \xrightarrow{k_2} P + P + h\nu.$$

The extent of excimer formation can be observed in the steady-state emission spectrum, where, in addition to the monomer (P^*) emission (370 to 400 nm), the excimer (P_2^*) emission gives rise to a broad band centered around 480 nm. Thus under pulsed excitation conditions, the fluorescence intensity due to the monomer and the excimer can be independently monitored as a function of time.

In homogeneous solutions, excimer formation follows second-order kinetics and the monomer and excimer intensity profile (change in population of P^* and P_2^* as a function of time) are (12, 17a)

$$I_m(t) = I_m(0)\exp[-(k_0 + k_e'[P])t] \quad [1a]$$

$$I_e(t) = \frac{I_m(0)k_e'[P]}{(k_2 - k_0 - k_e'[P])} \times [\exp[-(k_0 + k_e'[P])t] - \exp[-k_2 t]], \quad [1b]$$

where k_0 and k_2 (units of s^{-1}) are reciprocal lifetimes of P^* (in the absence of excimer formation) and P_2^* respectively; k_e' (units of $mole^{-1}\ s^{-1}$) is the second-order excimer formation rate constant; [P] is the concentration of pyrene.

The above rate laws predict that in homogeneous solutions the monomer intensity profile will be monoexponential with a slope that depends on the level of pyrene in the system. The excimer intensity profile, because k_2 is generally larger than $(k_0 + k_e'[P])$, will have an initial growth (when $k_2 t$ is comparable to $(k_0 + k_e'[P])t$) followed by a decline (when $k_2 t \gg (k_0 + k_e'[P])t$). The excimer decline will be controlled by the $\exp[-(k_0 + k_e'[P])t]$ term in Eq. [1b] and hence will be parallel to the monomer profile.

In fragmented media composed of micelles (or other aggregates of limited size in which pyrene is solubilized), the probability of the excited singlet state (P^*) of pyrene leaving one micelle and interacting with a ground state pyrene from another micelle during its excited lifetime is very low; the exit of pyrene from micelles is a millisecond phenomenon compared to its nanosecond fluorescence (11). Hence, the excimer formation of pyrene is essentially an intramicellar process. Only those micelles which contain more than one pyrene at the instant of flash excitation can give rise to excimers. In the time scale of the fluorescence, therefore, the micelles are considered as fixed solubilization sites with pyrene randomly distributed among them. The micellar system is viewed as groups of individual micelles with probe occupancies of 0, 1, 2, 3, . . . , etc. The relative size of each group is determined by the total number of probes available. This situation can be expressed mathematically by Poisson statistics (18) as

$$P_n = \bar{n}^n \exp(-\bar{n})/n!, \quad [2]$$

where P_n is the probability of micelles with n probes and $\bar{n}$ is the average number of probes per micelle.

The kinetic model to describe intramicellar excimer formation for the ensemble of micelles, MP_n, where $n = 1, 2, 3, \ldots$ is as follows (19):

$$MP_n \xrightarrow{+h\nu} MP^*P_{n-1}$$

excitation of ensemble,

$$MP^*P_{n-1} \xrightarrow{k_0} MP_n + h\nu$$

first-order radiative decay of monomer,

$$MP^*P_{n-1} \xrightarrow{(n-1)k_e} MP_2^*P_{n-2}$$

first-order intramicellar excimer formation,

$$MP_2^*P_{n-2} \xrightarrow{k_2} MP_n + h\nu$$

first-order radiative decay of excimer.

where k_0 and k_2 are the reciprocal lifetimes of P^* (in the absence of excimer formation) and P_2^* respectively. In this scheme, intramicellar excimer formation is first-order with a rate that increases as the number of probes in the micelle increases; k_e expresses the intramicellar encounter frequency of P^* and P (alternatively, $(n-1)k_e$ is the rate at which a micelle, $MP^*P_{(n-1)}$, converts to $MP_2^*P_{(n-2)}$).

The behavior of pyrene in a fragmented medium differs from that in homogeneous solution (infinite or continuous medium) in the following respects:

1. At low pyrene levels, the probability of a micelle containing more than one probe is negligible so that excimer formation does not occur. The monomer decay profile is monoexponential with a slope (k_0) corresponding to the radiative lifetime of P* ($t_0 = 1/k_0$) in the absence of excimer formation.

2. As the pyrene concentration increases, a fraction of the micelles will contain more than one probe. Excimer formation occurs in these micelles with the result that P* decay is enhanced. The monomer profile is therefore a sum of exponentials, each of which corresponds to the decay of P* in micelles having $n = 1, 2, 3, \ldots$. If excimer formation occurs rapidly, i.e., $k_e > k_0$, the monomer profile will contain an initial rapid decline due to decay of P* through excimer formation in micelles with $n > 1$, followed by a long-term single exponential component. This component, which corresponds to the radiative decay of P* in micelles with $n = 1$, is parallel to the curve at low pyrene concentrations (where no excimer formation occurs).

3. Unlike for the infinite medium case, the excimer profile for the fragmented medium case will not be parallel (after the initial growth) to the monomer profile.

These differences can be particularly useful in determining the structure of the microenvironment formed by the adsorbed surfactant molecules. A surface composed of individual surfactant aggregates of limited size is likely to behave as a fragmented medium. On the other hand, if the surfactant molecules form a large continuous environment, then the probe solubilized in this environment would probably behave as it does in homogeneous solutions.

Assumption of the intramicellar excimer formation kinetic model, and Poisson statistics for the probe distribution, leads to the following equation for the time dependence of monomer emission (19):

$$I_m(t) = I_m(0)\exp[-k_0 t + \bar{n}(\exp(-k_e t) - 1)], \quad [3]$$

where k_0 and k_e are as defined previously. $\bar{n}$ is the average occupation number and is given by

$$\bar{n} = [P]/[Agg] = [P] \times N/[C_t - CMC] \quad \text{for micelles,} \quad [4a]$$

$$= [P] \times N/[C_t - C_{eq}] \quad \text{for adsorbed layer,} \quad [4b]$$

where [P] = total pyrene concentration; N = aggregation number; [Agg] is the concentration of surfactant aggregates; [C_t − CMC] = concentration of micellized surfactant with C_t and CMC being the total surfactant concentration and critical micelle concentration respectively; [$C_t - C_{eq}$] = concentration of adsorbed surfactant with C_{eq} being the equilibrium concentration of surfactant (unadsorbed).

Analysis of the monomer decay profiles using Eq. [3] can yield $\bar{n}$ from which the surfactant aggregation numbers can be determined using Eq. [4a] or [4b].

Inherent in the derivation of Eq. [3] are several assumptions such as (i) complete solubilization of the probe, (ii) equal probability of occupation with no limit to occupation number for an aggregate, (iii) first-order kinetics to describe intramicellar excimer formation, and (iv) nonradiative dissociation of the excimer is negligible. The validity of these assumptions has been discussed in the literature (15b, 18, 19).

Intramolecular Excimer Formation of Dinaphthylpropane (DNP): Microviscosity of Environment

The extent of excimer formation as a measure of the local probe mobility has been utilized to determine the effective viscosity of microenvironments such as micelles (10, 11). As the viscosity of the medium increases, the

probe mobility is retarded with the result that the efficiency of excimer formation (which is diffusion limited) decreases. Although intermolecular excimer forming probes such as pyrene may be used for this purpose (20), the analysis, as suggested in the preceding discussion, is complicated by other factors such as probe distribution (18). A variation of this technique is the use of bichromophoric probes such as dinaphthylpropane, where excimer formation is exclusively unimolecular and statistical factors may be ignored (21). Experimentally the ratio of monomer to excimer intensities (at 342 and 420 nm for DNP) may be obtained from steady-state emission spectrum in solvents of known viscosity and the viscosity of the system under study compared on this scale. SDS micellar microviscosities of ~20–40 cp in the absence of additives have been reported using this technique (11). Although viscosities obtained in homogeneous solutions may not be strictly comparable to those in microenvironments, the technique is useful for monitoring structural changes (phase transitions) that occur within surfactant microenvironments such as micelles and adsorbed layers.

EXPERIMENTAL

MATERIALS

Alumina used in the present study was of 99% purity (Linde A grade, Union Carbide Corp.). The particle size was specified to be 0.3 μm with a BET surface area of 15 m^2/g by nitrogen adsorption. The point of zero charge determined by electrophoresis was at pH 8.4.

Sodium dodecyl sulfate (SDS) obtained from Fluka Chemicals was of 99% purity. Surface tension of solutions prepared from the as-received sample showed no detectable minimum so that the sample was used for subsequent tests without further purification.

Pyrene (Aldrich) was recrystallized from ethanol–water mixtures. Dinaphthylpropane was synthesized using a procedure described by Chandross *et al.* (22).

NaCl, HCl, and NaOH used were of ACS grade. All solutions were prepared in triply distilled, 10^{-6} mho conductivity water.

METHODS

Analytical Techniques

Dodecyl sulfate was analyzed by a two-phase technique involving titration of SDS against hexadecyltrimethylammonium bromide in chloroform with dimidium bromide-disulfine blue as endpoint indicator (23). Pyrene was analyzed by UV absorption at 333 nm using an absorption coefficient of 4.5×10^4 $mole^{-1}$ cm^{-1}.

Adsorption Experiments

A known weight of alumina (5 or 30 g) was equilibrated at pH 6.5 for 12 h with 150 ml of solution containing 0.1 *M* NaCl and a known amount of SDS. The pH of the suspension was adjusted with 0.1 *M* HCl at the start of the experiment and again 1 h before the end of the equilibration period. The suspension was stirred over a magnetic stirrer in a temperature bath maintained at 25°C.

Fifty milliliters of the final suspension was centrifuged and about 10 ml of the resulting supernatant was used for analysis. Some of the solids from the adsorption test were added to the remaining supernatant and the resulting diluted suspension was used for zeta potential measurements using a Lazer-Zee meter electrophoresis apparatus (Pen Kem Inc).

Fluorescence Experiments

Sample preparation. The same adsorption procedure was followed as in the experiments conducted in the absence of probe. Five grams of alumina was used in all tests. The SDS solutions used were prepared by adding a required volume of stock solution containing known concentrations of probe ($\sim 1 \times 10^{-3}$ *M* pyrene and 1×10^{-4} *M* DNP, respectively). The stock solutions were prepared by stirring pyrene or DNP crystals in 1×10^{-1} *M* SDS solutions for 24 h and filtering off the excess

probe. Stock solutions of lower probe concentrations were prepared by subsequent dilutions of the first stock with SDS solutions of equal concentration.

Steady-state experiments. Steady-state emission spectra were obtained using either a Spex Fluorolog or Perkin–Elmer LS-5 spectrophotometer. A portion of the adsorption sample was transferred to a 2-mm quartz cell. The resulting fluorescence emission spectrum was recorded and corrected for scattered incident light by scanning a blank sample that contained no probe. Pyrene- and DNP-containing samples were excited at 332 and 280 nm, respectively.

Fluorescence decay of pyrene. A PRA nanosecond flashlamp (nitrogen) and Ortec single-photon counting equipment and multichannel analyzer were used. The principles of single-photon counting for time-resolved data acquisition have been discussed elsewhere (24). The sample used for the steady-state emission experiments was also excited at 320 nm at a 45° angle of incidence for these tests. The monomer and excimer decay profiles were monitored at 383 and 480 nm, respectively. A pulse rate of 20 kHz and a timescale of 4.19 ns/channel were used.

For comparative studies, fluorescence studies with micellar solutions were conducted using air-saturated (no degassing) samples in 10-mm path length cells at normal incidence of excitation.

RESULTS AND DISCUSSION

ADSORPTION OF DODECYL SULFATE (SDS) ON ALUMINA

The adsorption isotherm of dodecyl sulfate on alumina at pH 6.5 in 0.1 *M* NaCl (Fig. 1a) exhibits features that are characteristic of anionic surfactant adsorption onto a positively charged oxide. The isotherm can be divided into four regions (6c, 6d). At low concentrations (Region I) the isotherm is linear with a slope of ~1. An abrupt transition from Region I to II occurs at $C_{eq} = 7.5 \times 10^{-5}$ *M* (adsorption density = 3×10^{-13} moles/cm^2) beyond which a marked increase in surfactant adsorption is observed. Region II extends linearly up to $C_{eq} = 2 \times 10^{-4}$ *M* (Ads. density = 7×10^{-11} moles/cm^2). Region III is characterized by a continuously decreasing slope even though adsorption continues to increase. The onset of the plateau (Region IV) is at $C_{eq} = 1.5 \times 10^{-3}$ *M* which also corresponds to the CMC of the bulk solution (monitored in the supernatants by the pinacyanol dye solubilization technique (25)).

The corresponding zeta potential behavior of alumina particles is found to correlate with the amount of adsorbed SDS as shown in Fig. 1b. In Region I, the potential is relatively constant and equal to that of alumina particles at pH 6.5 in the absence of SDS (+40 mV). A significant decrease in the positive potential is observed beyond the transition from Region I to II which correlates with the marked increase in anionic surfactant adsorption. The isoelectric point corresponding to the neutralization of the positively charged surface by the adsorbed anionic surfactant appears to coincide with the transition from Region II to III. Region III is therefore characterized by SDS adsorption resulting in a net negative potential at the surface. Constant negative potentials (−65 mV) are measured when the adsorption reaches its plateau level in Region IV.

The interpretation of the shape of the isotherm and corresponding zeta potential behavior has been reviewed in detail in the literature (6). Based on this information, the adsorption mechanisms giving rise to the above behavior can be stated as follows:

1. The slope of unity in Region I indicates that the anionic surfactant adsorbs as individual ions through electrostatic interaction with the positively charged surface.

2. The sharp increase in adsorption in Region II marks the onset of surfactant association at the surface through lateral interaction of the hydrocarbon chains.

3. The decreasing slope in Region III can be attributed to an increasing electrostatic hindrance to the surfactant association process following interfacial charge reversal.

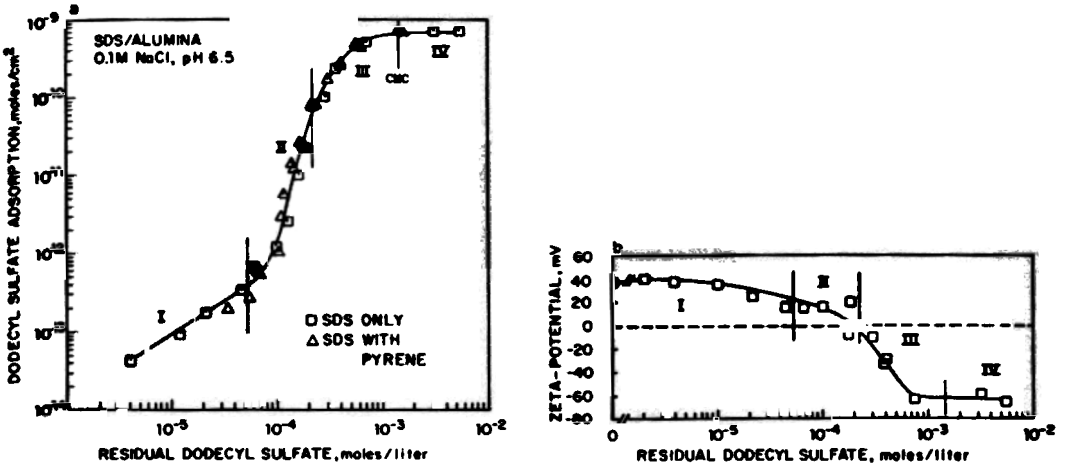

FIG. 1. (a) Adsorption isotherm of sodium dodecyl sulfate (SDS) on alumina at pH 6.5 in 10^{-1} *M* NaCl. (b) Zeta potential of alumina as a function of equilibrium concentration of SDS (designation of regions based on isotherm shape).

4. Plateau adsorption could correspond to either complete surface coverage or a value limited by constant surfactant monomer activity in solution as a result of bulk micellization. The prevailing situation would depend upon the extent to which the surface is charged through protonation and deprotonation of surface hydroxyls. Under the present conditions, the plateau can be interpreted as being CMC limited but also at or very near complete surface coverage. The latter is inferred from the plateau adsorption value (6.7×10^{-10} moles/cm^2) which indicates a densely packed monolayer (25 Å^2 molecular area for sulfate group) or a less densely packed bilayer (50 Å^2 molecular area).

The above description of the nature of the surfactant aggregation process at the surface and the structure of the adsorbed layer formed is, however, mostly hypothetical. In adsorption models, the aggregation process has been treated as a two-dimensional condensation that leads to the formation of monolayered- or bilayered-type surfactant assemblies termed hemimicelles (26) or admicelles (27). These assemblies are thought to occur in a localized (patchwise) manner due to the energetic heterogeneity of the surface (28); the positive sites are considered to be distributed into nonadjacent regions where surfactant condensation takes place. The validity of such assumptions and molecular models developed therefrom can be verified only through a direct probing of the adsorbed phase through spectroscopic methods.

FLUORESCENCE STUDIES ON ADSORBED LAYER OF SDS ON ALUMINA

Steady-state and transient experiments were used to obtain information on the microenvironment of SDS adsorbed on alumina under the experimental conditions mentioned above. Comparative studies were also performed using SDS micellar solutions in 0.1 *M* NaCl.

Local Polarity

Emission spectra obtained for pyrene in alumina slurries containing adsorbed SDS showed the characteristic pyrene fluorescence fine structure with respect to the positions of the various vibrionic bands. The change in intensity ratio, $I3/I1$, of pyrene in SDS solutions of varying concentrations in the presence of 0.1 *M* NaCl is given in Fig. 2a. The ratio changes sharply at CMC (1.5×10^{-3} *M*) from a value of 0.6, corresponding to pyrene in

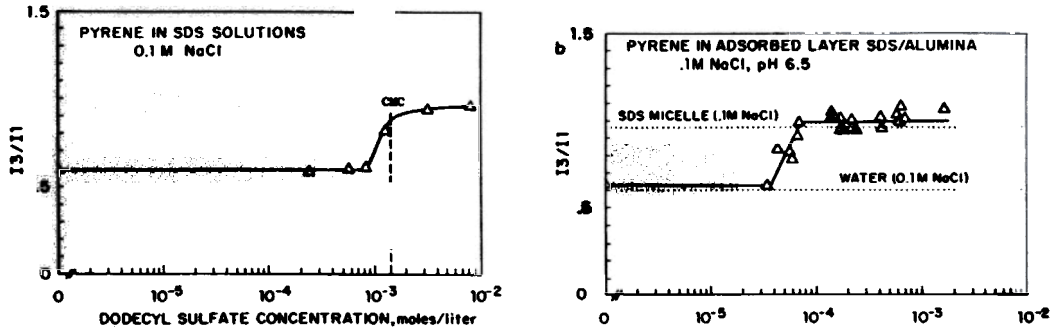

FIG. 2. (a) $I3/I1$, fluorescence parameter of pyrene in sodium dodecyl sulfate (SDS) solutions in 10^{-1} M NaCl (λ_3 = 383 nm, λ_1 = 374 nm). (b) $I3/I1$, fluorescence parameter of pyrene in SDS/alumina slurries.

aqueous media, to a value of 1.0, corresponding to pyrene solubilized in SDS micelles.

Figure 2b shows the behavior of pyrene in SDS–alumina slurries as a function of SDS equilibrium concentration at points corresponding to the adsorption isotherm in Fig. 1a. In Regions II, III, and IV (near CMC), no pyrene was detected in the supernatants of the slurries, which suggests that pyrene is completely solubilized in the adsorbed layer. In Region I, almost all the pyrene was present in aqueous solution in the supernatant,[1] suggesting that pyrene by itself does not strongly adsorb on alumina. Also, the adsorption isotherm in the presence and absence of pyrene (Fig. 1a) was identical so that the adsorption of SDS is not significantly influenced by the presence of pyrene at the added levels (10^{-7}–10^{-5} M).

The data in Fig. 2b show an abrupt change in the local polarity of the probe from aqueous environment to a relatively nonpolar, micelle-type environment. This change occurs in a region that is well below the CMC (where no micelles are present) and that approximately coincides with the transition in the adsorption isotherm from Region I to II. Interestingly, the $I3/I1$ values of the probe are also relatively constant (~1.0) throughout most of Region II and up to Region IV and hence independent of surface coverage. The above results suggest the existence of solubilization sites for pyrene on the surface that are formed by micellelike association of hydrocarbon chains. Clearly, such aggregation takes place significantly only in Region II and above. In addition, the microenvironment formed by the associated surfactant appears to be similar in nature throughout the entire adsorption isotherm.

Microviscosity

Typical emission spectra obtained for the intramolecular excimer forming probe, dinaphthylpropane, in micellar solutions and in the adsorbed layer are shown in Fig. 3a. It can be seen that the extent of excimer formation in the adsorption sample (I_m/I_e = 4) is significantly lower than that in the micellar solution (I_m/I_e = 1.7). The mobility of the probe can therefore be considered to be more restricted in the adsorbed layer than in the micelle.[2]

[1] The concentrations of pyrene added for the polarity tests in Region I were below the aqueous solubility limit. The emission intensities were weak when pyrene was mostly present in solution and increased significantly when it was solubilized in the adsorbed layer.

[2] In order to ascertain that the I_m/I_e ratio measured in the solid slurries was not due to some intrinsic artifact such as scattering of light, a control experiment was conducted. An SDS micellar solution containing DNP was added to silica particles (on which SDS did not adsorb) and the resulting DNP spectrum was recorded. The I_m/I_e in this sample was the same as that of the SDS micellar solution (except that the emission intensity was much lower). The presence of the solid, thus, did not interfere with the measurement; the response of DNP reflected the fact that it was present exclusively in micelles. Hence, it can be concluded that the I_m/I_e value of DNP in the SDS/alumina system reflects its environment in the adsorbed layer.

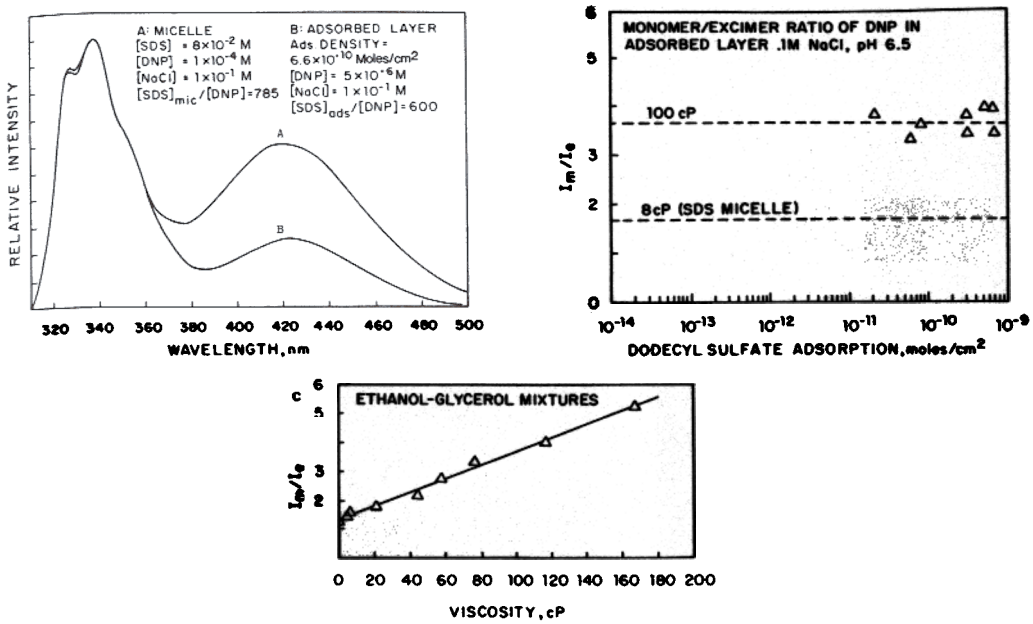

FIG. 3. (a) Spectrum A: Dinaphthylpropane (DNP) fluorescence in SDS micellar solution ($[SDS]_{mic}/[DNP]$ = ratio of micellized SDS to DNP). Spectrum B: DNP fluorescence in SDS/alumina slurry ($[SDS]_{ads}/[DNP]$ = adsorbed SDS to DNP). (b) Monomer to excimer ratio (I_m/I_e) of dinaphthylpropane (DNP) in SDS/alumina slurries as a function of SDS adsorption (λ_m = 340 nm, λ_e = 420 nm). (c) Monomer to excimer ratio (I_m/I_e) of dinaphthylpropane (DNP) in ethanol–glycerol mixtures (viscosities measured by capillary flow method).

Similar measurements as a function of adsorption density (Fig. 3a) indicate that the extent of excimer formation is independent of the surface coverage in the range of adsorption densities measured (Region II to IV).

The I_m/I_e response of DNP was calibrated in ethanol–glycerol mixtures of known viscosities (Fig. 3b). Based on this scale the adsorbed layer and micelle viscosities are 90–120 and 8 cP, respectively. The high microviscosity in the adsorbed layer suggests that the surface phase is highly structured and almost rigid. Furthermore, no significant structural rearrangements occur with increase in surface coverage (in the range of adsorption densities studied); i.e., it is possible that the associated structures that form at lower surface coverages are already in a densely packed state which cannot be compressed any further. Such a situation can be expected if condensed surfactant assemblies exist on the surface.

Fluorescence Decay of Pyrene in SDS Solutions

The fluorescence decay behavior of pyrene in an SDS micellar solution in 0.1 *M* NaCl (Fig. 4) is typical for that in fragmented media. Curve A is the monomer profile obtained under nonexcimeric conditions, i.e., at low levels of pyrene (indicated as the ratio of SDS to pyrene). The radiative lifetime of pyrene, $1/k_0$, in SDS micelles, calculated from the slope of this monoexponential curve, is 175 ns. Curve B is the monomer profile when excimer formation occurs (see emission spectrum) and Curve C is the corresponding excimer profile. Computer fitting of curve B (see Appendix) to Eq. [3] yields the excimer formation rate, k_e, and the mean occupation number, $\bar{n}$. The aggregation number, N, for the SDS micelle in 0.1 *M* NaCl is calculated using Eq. [4a] to be 118. The results are summarized in Table I.

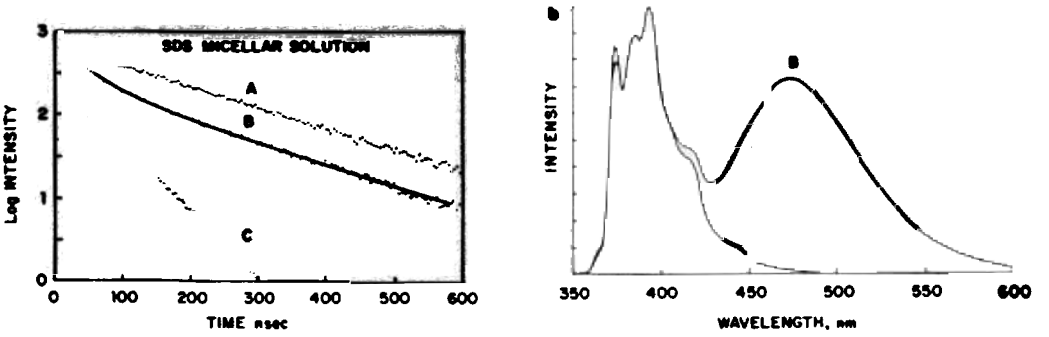

FIG. 4. (a) Pyrene monomer and excimer decay profiles in SDS micellar solutions; [SDS] = 8.2×10^{-2} *M*, [NaCl] = 1×10^{-1} *M*, CMC = 1.5×10^{-3} *M*. Pyrene levels are indicated as ratio of micellized SDS to pyrene; (monomer emission monitored at 383 nm, excimer emission at 480 nm). Curve A: Monomer emission profile for SDS/PY = 2160. Curve B: Monomer emission profile for SDS/Py = 108. Curve C: Excimer emission profile for SDS/PY = 108. (b) Pyrene fluorescence spectra in SDS micellar solutions corresponding to conditions in Fig. 4a. Spectrum A: SDS/PY = 2160; Spectrum B: SDS/PY = 108.

Fluorescence Decay of Pyrene in Adsorbed Layer

Typical decay profiles of pyrene in the adsorbed layer for the indicated adsorption densities are given in Figs. 5–7. Included in each figure are the monomer profile (Curves A and B) at two pyrene levels (indicated as SDS/PY, the number of surfactant molecules per probe in adsorbed layer) and the corresponding emission spectra. The excimer profiles at the higher pyrene levels are also given (Curve C).

Examination of the monomer and excimer profiles obtained for the adsorbed layer samples and comparison with that obtained for the micellar solution suggest the following:

1. Under excimeric conditions (Curve B), the profiles obtained in the adsorbed layer are multiexponential suggesting that pyrene, like in micelles, reports a fragmented-type structure. However, the initial declines of the monomer profiles in each of the adsorbed layer samples are less steep than those in the micellar solution implying that excimer formation occurs more slowly in the adsorbed layer than in the micelle. It should be noted that although the highest adsorption density sample exhibits fragmented medium properties, it also tends to exhibit homogeneous environment properties; the monomer profile is nearly monoexponential and the excimer and monomer declines are almost parallel. A homogeneous type environment could be expected near the plateau adsorption levels since the adsorption density corresponds closely to complete coverage of the surface as discussed earlier.

2. That the excimer formation occurs more slowly in the adsorbed layer than in the micelle can also be qualitatively inferred from the "parallelism" of the corresponding monomer and excimer profiles; a larger k_e results in a greater deviation of the monomer and excimer curves in accordance with the fragmented medium model. In all adsorption cases, the

TABLE I

Summary of Kinetic Analysis of Pyrene Excimer Formation; SDS Micelle (0.1 *M* NaCl)

SDS concn. (moles/liter)	CMC	SDS/PY	$1/k_0$, ns	k_e, s^{-1}		N
8.2×10^{-2}	1.5×10^{-3}	108	175	1.4×10^{7}	1.10	118

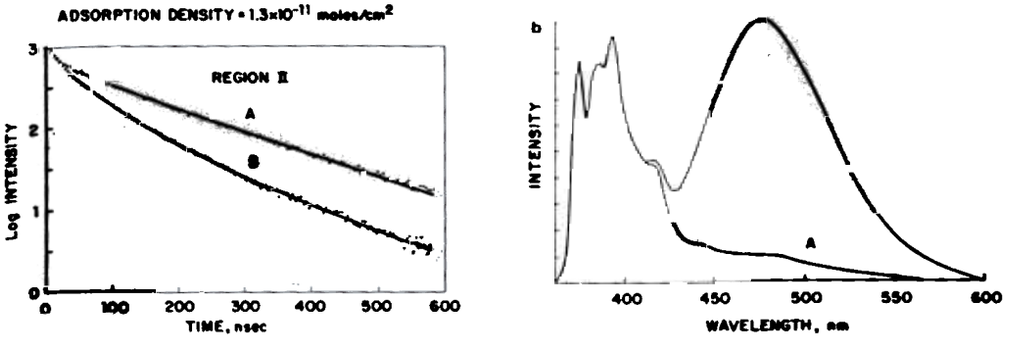

FIG. 5. (a) Pyrene monomer and excimer decay profiles in SDS/alumina adsorbed layer; pyrene levels indicated as ratio of adsorbed SDS to pyrene; Ads. density = 1.3×10^{-11} moles/cm^2, $[SDS]_{eq} = 1.4 \times 10^{-4}$ M/l, pH 6.5, [NaCl] = 1×10^{-1} M, (monomer emission at 383 nm, excimer emission at 480 nm). Curve A: Monomer profile for SDS/PY = 520. Curve B: Monomer profile for SDS/PY = 52. Curve C: Excimer profile for SDS/PY = 52. (b) Pyrene fluorescence spectra in SDS/alumina adsorbed layer corresponding to conditions in Fig. 5a. Spectrum A: SDS/PY = 520; Spectrum B: SDS/PY = 52.

monomer and excimer curves deviate less from each other than do the corresponding curves in the micellar solution, again suggesting that excimer formation is slower in the adsorbed layer.

Curves A and B were fitted using Eq. [3] in order to obtain k_0, k_e, and $\bar{n}$ (see Appendix). These results are summarized in Table II. Aggregation numbers, N, calculated via Eq. [4b] are also included. The reproducibility in these calculated parameters was checked by duplicate tests (5 and 7, 14 and 15 in Table II) as well as tests conducted at varying pyrene levels but at the same adsorption density (4 and 5, 6 and 7, 9 and 10, 13 and 14 in Table II). k_e and N were reproducible to about 10% except at low adsorption densities. At low adsorption densities the inaccuracies in determining adsorption densities and hence SDS/PY, as well as the weaker emission intensities, contribute to errors of about 20% in these parameters. Within these experimental errors, k_e and N

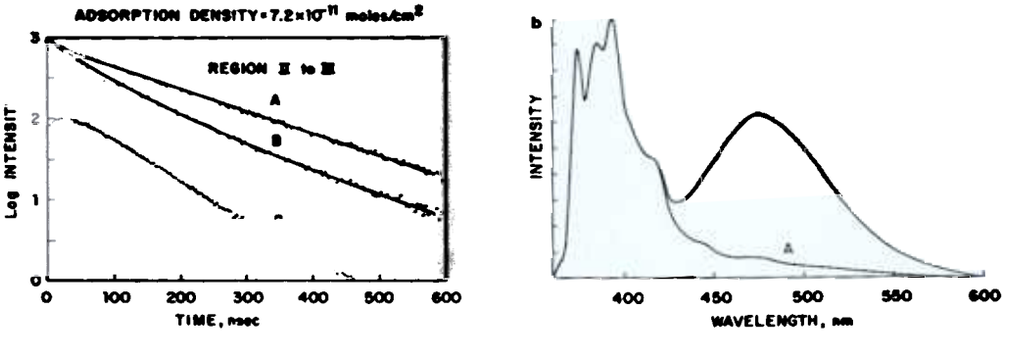

FIG. 6. (a) Pyrene monomer and excimer decay profiles in SDS/alumina adsorbed layer; pyrene levels indicated as ratio of adsorbed SDS to pyrene; adsorption density = 7.2×10^{-11} moles/cm^2, $[SDS]_{eq} = 2.2 \times 10^{-4}$ M, other conditions as in Figure 5a. Curve A: Monomer profile for SDS/PY = 1090. Curve B: Monomer Profile for SDS/PY = 109. Curve C: Excimer profile for SDS/PY = 109. (b) Pyrene fluorescence spectra in SDS/alumina adsorbed layer corresponding to conditions in Fig. 6a. Spectrum A: SDS/PY = 1090; Spectrum B: SDS/PY = 109.

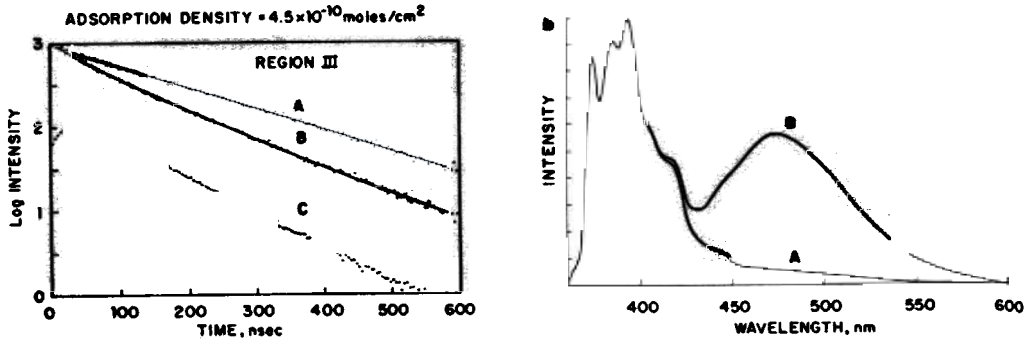

FIG. 7. (a) Pyrene monomer and excimer decay profiles in SDS/alumina adsorbed layer; pyrene levels indicated as ratio of adsorbed SDS to pyrene; Ads. density = 4.5×10^{-10} moles/cm^2, $[SDS]_{eq} = 5.8 \times 10^{-4}$ *M*, other conditions as in Figure 5a. Curve A: Monomer profile for SDS/PY = 1390. Curve B: Monomer profile for SDS/PY = 139. Curve C: Excimer profile for SDS/PY = 139. (b) Pyrene fluorescence spectra in SDS/alumina adsorbed layer corresponding to conditions in Fig. 7a. Spectrum A: SDS/PY = 1390; Spectrum B: SDS/PY = 139.

are independent of pyrene concentration at a particular adsorption density in accordance with the prediction of the kinetic model used here.

Monomer lifetime. The monomer lifetimes ($1/k_0$) for samples obtained in Region II and above of the adsorption isotherm in Fig. 1a, range from 158 to 175 ns[3] with no significant trend as a function of adsorption density. These lifetimes are comparable to that of pyrene in SDS micelles (175 ns) but are larger than that of pyrene in water (135 ns). These lifetimes suggest an environment for pyrene in the adsorbed layer that is similar to that of micelles.

Excimer formation rate. The values of k_e for the adsorbed layer are, (depending on the adsorption density), 2 to 8× smaller than that for the micelle. The rate constant, k_e, has been defined as the intramicellar encounter frequency of an excited-state pyrene with an unexcited-state pyrene which, in turn, depends upon the mobility of the probe in its environment. The range obtained for the rate of excimer formation here is thus supporting evidence that the adsorbed layer is more viscous compared to the micelle. This is in agreement with the conclusion from the extent of excimer formation of DNP presented earlier.

The data in Table II also indicate a decreasing trend for k_e with increase in adsorption density with particularly small values being determined at high surface coverages. This trend in k_e is not likely to result from microviscosity effects since no significant differences in microviscosity were observed as a function of adsorption density (DNP measurements). It is to be noted that in addition to local viscosity, other factors such as shape and dimensions of the aggregates can affect the *intermolecular* excimer formation rate. These factors affect the local concentration of pyrene (interprobe distance) and hence the time of encounter between P and P*. Indeed the lower k_e values in Table II were obtained in larger aggregates. The observed change in k_e as a function of adsorption density is thus attributed to the increase in average interprobe distance resulting from the growth of aggregates.

Aggregation number. The change in aggregate size with adsorption is shown in Fig. 8. The average aggregation number, *N*, measured

[3] The ~20-ns variation in lifetimes was for experiments conducted on different days; a much smaller variation was observed for tests run on the same day. This effect was subsequently traced to day-to-day room temperature fluctuations during the decay measurements. For all the data in Table II, Curves A and B were obtained on the same day and hence had the same k_0.

TABLE II

Summary of Kinetic Analysis of Pyrene Excimer Formation; SDS/Alumina Adsorbed Layer (pH 6.5, 0.1 *M*/l NaCl)

Test No.	Adsorption density (moles/cm²)	SDS/PY	$1/k_0$, ns	k_e, s^{-1}	$\bar{n}$	N
1	1.2×10^{-12}	39	[a]163	7.3×10^{6}	1.68	66
2	3.0×10^{-12}	21	[a]163	6.6×10^{6}	2.35	49
3	5.0×10^{-12}	74	163	7.2×10^{6}	1.64	121
4	1.2×10^{-11}	128	163	6.6×10^{6}	1.06	136
5	1.3×10^{-11}	52	160	6.0×10^{6}	2.04	106
6	1.3×10^{-11}	275	158	6.5×10^{6}	0.53	146
7	1.2×10^{-11}	55	158	6.7×10^{6}	1.92	105
8	2.3×10^{-11}	71	158	6.2×10^{6}	1.80	128
9	6.9×10^{-11}	260	163	5.1×10^{6}	0.65	169
10	7.2×10^{-11}	109	162	4.8×10^{6}	1.44	157
11	7.6×10^{-11}	117	172	4.4×10^{6}	1.47	172
12	1.7×10^{-10}	132	163	4.6×10^{6}	1.49	196
13	4.4×10^{-10}	336	175	2.4×10^{6}	0.74	250
14	4.5×10^{-10}	139	175	2.4×10^{6}	1.86	258
15	4.6×10^{-10}	146	163	2.5×10^{6}	1.77	258
16	6.6×10^{-10}	123	168	1.8×10^{6}	2.91	356

[a] $1/k_0$ was set at 163 ns.

at particular adsorption densities is indicated along the isotherm. In general, the size of aggregates increases with adsorption density with relatively small aggregates existing near the onset of Region II (the difference in N of 49 and 60, based on the experimental uncertainties, is not significant). The aggregates in Region II appear to be relatively uniform in size (121–128) while in Region III a marked growth in aggregates (166–356) is observed as adsorption density increases. The implications of this overall behavior in terms of the evolution of the adsorbed layer are discussed below and shown schematically in Fig. 9.

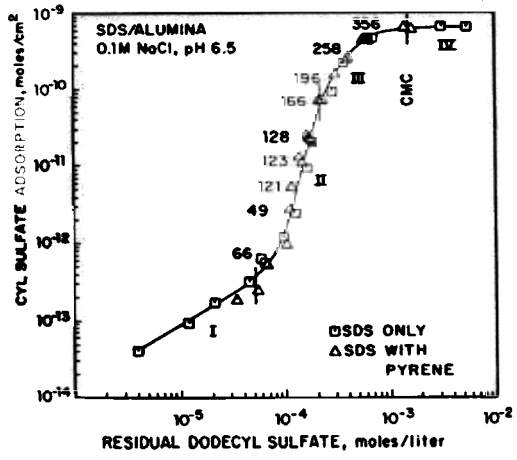

FIG. 8. Surfactant aggregation numbers as function of adsorption density (average number at each adsorption point shown along isotherm).

1. In Region I, no significant aggregation takes place and adsorption is likely to be due to electrostatic attraction of individual surfactant ions.

2. Adsorption in Region II and above occurs through the formation of surfactant aggregates of limited size.

3. In Region II, where the surface is essentially bare and sufficient number of positive sites are available (zeta potential is positive), increase in adsorption is achieved mostly by increasing the number of aggregates; a constant aggregation number implies that the number density of aggregates increases with increase in adsorption.

4. The transition from Region II to III marks the point at which most of the positive sites are filled since the zeta potential reverses in sign at this point. Adsorption in Region III is therefore likely to occur through the growth

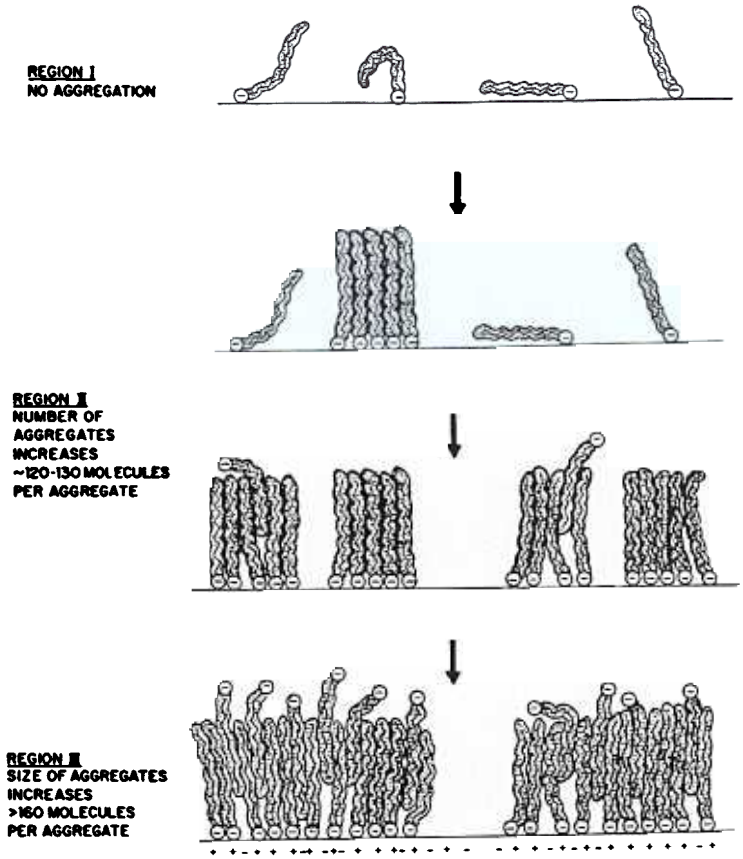

FIG. 9. Schematic representation of the correlation of surface charge and growth of aggregates for the various regions of the adsorption isotherm.

of existing aggregates rather than through the formation of new ones. The growth of these aggregates can be expected to be electrostatically hindered. This hindrance to the aggregation process results in the continuously decreasing slope for the adsorption isotherm; higher surfactant chemical potentials (concentrations) are required to offset the electrical repulsion experienced by the adsorbing molecules. Surfactant adsorption in Region III is also likely to occur with a reverse orientation as illustrated in Fig. 9 since there is an insignificant number of positive sites on the surface.

CONCLUSIONS

The fluorescence analysis of the adsorbed layer formed by dodecyl sulfate on alumina is in agreement with the basic concepts of hemimicellization. The surfactant aggregation occurs above a critical concentration (or adsorption density) that is marked by a sharp increase in adsorption and proceeds through the formation of highly organized and finite-sized assemblies even at relatively low surface coverages.

The surface charge appears to have an influence on the evolution of the surface aggregates as a function of surface coverage. In Region II when the surface is positively charged, relatively uniform-sized aggregates (120–130) are measured on the surface. A corollary of this is that adsorption in this region occurs by increasing the number of aggregates on the positive sites of the particle. When the positive charge on the mineral is neutralized, the energetic situation favors the growth of existing

aggregates rather than the formation of new aggregates. Thus in Region III, the size of aggregates increases significantly with adsorption density (166–356).

The present study shows that fluorescence spectroscopy, when used in conjunction with other techniques, is a powerful tool for elucidating the structure of surfactant adsorbed layers at the solid–solution interface.

APPENDIX

Fitting Procedure for Monomer Decay Profiles Using Eq. [3]

Equation 3,

$$I_m(t) = I_m(0)\exp[-k_0 t + \bar{n}(\exp(-k_e t) - 1)],$$

was fitted using the Marquardt–Levenberg nonlinear regression algorithm which involved minimization of the weighted sum of squares (SSQ):

$$\mathrm{SSQ} = \sum_i^N W_i(t)F_i^o(t) - F_i^c(t)]^2$$

where, W_i, the weight = $1/F_i^o(t)$; $F_i^o(t)$ and $F_i^c(t)$ are the observed and calculated number of counts, respectively.

Goodness of fit was checked by examining the (i) sum of squares, (ii) the fitted curve, and (iii) the weighted residuals, $1/[F_i^o(t)^{1/2}] \times [F_i^o(t) - F_i^c(t)]$. n, k_0, k_e were obtained by fitting Curves A and B simultaneously. For example, suppose Curve A was obtained with a 10× dilution in pyrene with respect to Curve B, then the equations fitted were

$$I_m(t) = I_m(0)\exp[-k_0 t + (\bar{n}/10)(\exp(-k_e t) - 1)]$$

for A,

$$I_m(t) = I_m(0)\exp[-k_0 t + \bar{n}(\exp(-k_e t) - 1)]$$

for B.

This procedure was found to be necessary because the pyrene levels for most of the adsorbed layer samples could not be lowered enough to ensure no excimer formation.

The zero time channel was taken as the channel in which the monomer intensity was maximum. The lamp profile extended up to about 25 ns. Fitting was begun from 50 ns without deconvolution. A background noise level corresponding to the last 25 channels was subtracted from the actual data. The noise level was generally less than 1% of the maximum intensity.

ACKNOWLEDGMENTS

The authors gratefully acknowledge the assistance of Dr. K. P. Ananthapadmanabhan, Dr. P. L. Kuo, Dr. C. V. Kumar, Dr. Ian Gould, Dr. Lei, and Dr. K. Arora at various stages of this work. This work was supported by NSF(CPE 82-01216).

REFERENCES

1. (a) Aplan, F. F., and Fuerstenau, D. W., (Ed.), "Froth Flotation." AIME, New York, 1962; (b) Somasundaran, P., *AIChE Symp. Ser.* **71**, 1 (1975).
2. Schwuger, M. J., "Anionic Surfactants," Surfactant Science Series, (E. H. Lucassen-Reynders, Ed.), Vol. 11, Dekker, New York, 1981.
3. (a) Hanna, H. S., and Somasundaran, P., "Improved Oil Recovery by Surfactant and Polymer Flooding," (D. O. Shah and R. S. Schecter, Eds.), Academic Press, New York, 1977; (b) Somasundaran, P., and Chandar, P., "Solid-Liquid Interactions in Porous Media," pp. 411–428. Technip, Paris, 1985.
4. Shilling, G. J., and Bright, G. S., *Lubrication* **63**, 13 (1977).
5. (a) Somasundaran, P., Healy, T. W., and Fuerstenau, D. W., *J. Phys. Chem.* **68**, 3562 (1964); (b) Hough, D. B., and Rendall, H. M., "Adsorption From Solution at the Solid-Liquid Interface," (G. D. Parfitt and C. H. Rochester, Eds.), Academic Press, New York, 1983; (c) Fuerstenau, D. W., *Trans. AIME.* December, 1365 (1957); (d) Somasundaran, P., Chandar, P., and Chari, K., *Colloids Surf.* **8**, 0, (1983); (e) Partyka, S., Zundhemer, M., Zaini, S., Keh, E., and Braun, B., "Solid-Liquid Interactions in Porous Media," pp. 509–522. Technip, Paris, 1985.
6. (a) Somasundaran, P., and Fuerstenau, D. W., *J. Phys. Chem.* **70**, 90 (1966); (b) Scamerhorn, J. F., Schecter, R. S., and Wade, W. H., *J. Colloid Interface Sci.* **85**, 0, (1982); (c) Harwell, J. H., "PhD Thesis." University of Texas at Austin, 1983; (d) Somasundaran, P., Middleton, R., and Viswanathan, K. V., "Structure and Performance Relationship in Surfactants," (M. J. Rosen, Ed.), pp. 270–290. ACS Symposium Series, Washington DC, 1984; (e) Chander, S., Fuerstenau, D. W., and Stigter, D., "Adsorption From Solution," (R. H. Ottewill, C. H. Rochester, and A. L. Smith, Eds.), pp. 197–

211. Academic Press, New York, 1983; (f) Wakamatsu, T., and Fuerstenau, D. W., "Adv. Chemistry Series," No. 79, pp. 161–172. ACS, New York.
7. Peck, A. S., Raby, L. H., and Wadworth, M. E., *Trans. AIME* **238**, 301 (1966).
8. Passaglia, E., Stromberg, R. R., and Kruger, J., (Eds.), "Ellipsometry in the Measurement of Surfaces and Thin Films." Symposium Proceedings, Nat. Bur. Standards, Miscellaneous Publication, No. 256.
9. (a) Turro, N. J., "Modern Molecular Photochemistry." Benjamin/Cummings, Menlo Park, CA, 1978; (b) Wehry, E. L., (Ed.), "Modern Fluorescence Spectroscopy," Vol. 2, Plenum, New York, 1976; (c) Thomas, J. K., "The Chemistry of Excitation at Interfaces," ACS Monograph, ACS, Washington DC, 1984.
10. (a) Turro, N. J., Gratzel, M., and Braun, A. M., *Angew. Chem. Int. Ed. Engl.* **19**, 675 (1980); (b) Gratzel, M., and Thomas, J. K., "Modern Fluorescence Spectroscopy," (E. L. Wehry, Ed.), pp. 169–213. Plenum, New York, 1976.
11. Singer, L. A., "Solution Behavior of Surfactants," (K. L. Mittal and E. J. Fendler, Eds.), Vol. 1, pp. 73–112. Plenum, New York.
12. Levitz, P., van Damme, H., and Keravis, D., *J. Phys. Chem.* **88**, 2228 (1985).
13. (a) Nakajima, A., *Bull. Chem. Soc. Jpn.* **44**, 3272 (1971); (b) Nakajima, A., *J. Lumin.* **11**, 429 (1976); (c) Nakajima, A., *J. Mol. Spectrosc.* **61**, 467 (1976); (d) Dorance, R., and Hunter, T., *J. Chem. Soc. Faraday Trans.* **68**, 1312 (1972); (e) Kalyanasundaram, K., and Thomas, J. K., *J. Chem. Soc. Faraday Trans.* **99**, 1312 (1977).
14. (a) Dong, D. C., and Winnik, M. A., *Photochem. Photobiol.* **35**, 17 (1982); (b) Lianos, P., and Georghiou, S., *Photochem. Photobiol.* **30**, 355 (1979).
15. (a) Kalayansundaram, K., and Thomas, J. K., *J. Amer. Chem. Soc.* **97**, 3915 (1975); (b) Lianos, P., Lang, J., Strazielle, C., and Zana, R., *J. Phys. Chem.* **86**, 1019 1982; (c) Ananthapadmanabhan, K. P., Goddard, E. D., Kuo, P. L., and Turro, N. J., *Langmuir* **1**, 352 (1985).
16. (a) Riegelman, S., Aelawala, N. A., Hrenoff, M. K., and Strait, L. A., *J. Colloid Sci.* **13**, 208 (1958); (b) Gratzel, M., Kalyanasundaram, K., and Thomas, J. K., *J. Amer. Chem. Soc.* **96**, 7869 (1974); (c) Turro, N. J., and Kuo, P. L., *Langmuir* **1**, 170 (1985); (d) Mukerjee, P., "Solution Chemistry of Surfactants," (K. L. Mittal and E. J. Fendler Eds.), Plenum, New York.
17. (a) Birks, J. B., "Photophysics of Aromatic Molecules," Macmillan Co., New York, 1970; (b) Forster, Th., and Selinger, B. K., *Z. Naturforsch. A* **19**, 38 (1964); (c) Hauser, M., and Klein, U., *Z. Phys. Chem.* **78**, 32 (1972); (d) Hauser, M., and Klein, U., *Acta Phys. Chem.* **19**, 363 (1973).
18. (a) Infelta, P. P., and Gratzel, M., *J. Phys. Chem.* **70**, 179 (1979); (b) Yekta, A., Aikawa, M., and Turro, N. J., *Chem. Phys. Lett.* **63**, 543 (1979).
19. Atik, S., Nam, M., and Singer, L., *Chem. Phys. Lett.* **67**, 75 (1979).
20. Pownall, H. J., and Smith, L. C., *J. Amer. Chem. Soc.* **95**, 3136 (1973).
21. (a) Turro, N. J., Aikawa, M., and Yekta, A., *J. Amer. Chem. Soc.* **101**, 772 (1979); (b) Emert, J., Behrens, C., and Goldenberg, M., *J. Amer. Chem. Soc.* **101**, 771 (1979); (c) Zachariasse, K., *Chem. Phys. Lett.* **57**, 429 (1978).
22. Chandross, E. A., and Dempster, C. J., *J. Amer. Chem. Soc.* **92**, 3586 (1970).
23. Reid, V. W., Longman, G. F., and Heinherth, E. *Tenside* **5**, 90 (1968).
24. Lakowicz, J. R., "Principles of Fluorescence Spectroscopy." Plenum, New York, 1983.
25. Mukerjee, P., and Mysels, K. J., *J. Amer. Chem. Soc.* **77**, 2937 (1955).
26. (a) Gaudin, A. M., and Fuerstenau, D. W., *Min. Eng.* **7**, 66 (1955); (b) Gaudin, A. M., and Fuerstenau, D. W., *Trans. AIME* **202**, 66 (1955).
27. Harwell, J. H., Hoskins, J. C., Schecter, R. S., and Wade, W. H., *Langmuir* **1**, 251 (1985).
28. Rakotonarivo, E., Bottero, J. Y., Cases, J. M., and Fiessinger, F., *Colloids Surf.* **9**, 273 (1984).